Parametric amplification in Josephson junction embedded transmission lines

O. Yaakobi,[1,*] L. Friedland,[2] C. Macklin,[3] and I. Siddiqi[3]
[1]*INRS-EMT, 1650 Boul. Lionel Boulet, Varennes, Quebec, J3X 1S2 Canada*
[2]*Racah Institute of Physics, The Hebrew University, Jerusalem 91904, Israel*
[3]*Quantum Nanoelectronics Laboratory, Department of Physics, University of California, Berkeley, California 94720, USA*
(Received 3 January 2013; revised manuscript received 26 February 2013; published 1 April 2013)

An electronic transmission line that contains an array of nonlinear elements (Josephson junctions) is studied theoretically. A continuous nonlinear wave equation describing the dynamics of the node flux along the transmission line is derived. It is shown that due to the nonlinearity of the system, a mixing process between four waves with different frequencies is possible. The mixing process can be utilized for amplification of weak signals due to the interaction with a strong pump wave. An analytical solution for the spatial evolution of the wave amplitudes is derived, and found to be in excellent agreement with the results of numerical computations. Simulations of realistic parameters show that the power gain can exceed 20 dB over a bandwidth of more than 2 GHz.

DOI: 10.1103/PhysRevB.87.144301 PACS number(s): 84.30.Le, 74.81.Fa, 85.25.−j, 05.45.−a

I. INTRODUCTION

Recent progress in the development of near quantum-noise-limited microwave amplifiers has enabled ultrasensitive detection in radio astronomy[1] and real-time monitoring of quantum bits.[2,3] Superconducting parametric amplifiers,[4–8] in particular, have demonstrated reliable, low-noise operation with power gain in excess of 20 dB and bandwidth ranging from 1–10 MHz.[9–13] These amplifiers, however, comprise a single Josephson junction or an array of junctions in a resonant cavity which ultimately limits the bandwidth and dynamic range. The use of a single resonant cavity also implies that these devices must operate in a reflection geometry, requiring the use of lossy, bulky microwave circulators between the amplifier and the system under measurement. The need for circulators has become a limiting factor on measurement sensitivity in some recent experiments on quantum-limited measurement[3,14] and has also prevented on-chip, large-scale integration of these amplifiers.

We consider an architecture based on a nonlinear transmission line comprising capacitively shunted Josephson junctions. Such traveling wave amplifiers have been addressed in previous theoretical proposals[15,16] without a complete nonlinear treatment of the dynamics of the transmission line or discussion of the mode matching conditions required for efficient four-wave mixing. Operation of a prototype device has also been reported using chains of Josephson junctions,[17] although this device was operated as a reflection amplifier and did not achieve impedance matching to 50 Ω. Operation of a device using the kinetic inductance of a thin superconducting transmission line has also been recently demonstrated.[18] We develop a detailed theoretical model to calculate the amplifier gain as a function of device length for experimentally relevant parameters.

The paper is organized as follows: In Sec. II we derive a continuous nonlinear wave equation describing the dynamics of the node flux along the transmission line, and present the coupled envelope equations of the degenerate four-wave mixing process. In Sec. III, we analyze the problem under the strong pump assumption without dissipation, present numerical solutions of the envelope equations, and compare with the approximate analytic solutions. Finally, our results are summarized in Sec. IV. The derivation of the coupled envelope equations (that are presented in Sec. II) is described in detail in the Appendix.

II. NONLINEAR WAVE EQUATION

In this section, we derive the nonlinear wave equation describing the dynamics of a capacitively shunted Josephson junction transmission line (Fig. 1). This circuit model can be realistically implemented in a microstrip-geometry transmission line, wherein the linear inductance of the microstrip per unit cell can be made negligible compared to the Josephson inductance by using a relatively wide microstrip trace and short unit cell spacing. We proceed by writing the current conservation relation, capacitor current-voltage relation, and Josephson current for each cell. Next, we use the continuum approximation, leading to the desired wave equation. In the following, we assume that the capacitance C is the same along the transmission line, but the capacitance C_J may vary from cell to cell. The current conservation in each cell reads

$$I_n = I_{(C_J),n} + I_{L,n}. \tag{1}$$

The current in capacitor C_J,n is related to the voltages V_n and V_{n+1} by the derivative,

$$I_{(C_J),n} = -C_J \frac{d}{d\tilde{t}}(V_{n+1} - V_n), \tag{2}$$

where $\tilde{t}$ denotes time. We use the usual magnetic flux definition,

$$V_{n+1} - V_n = -\frac{d\Phi_n}{d\tilde{t}}, \tag{3}$$

and the expression for the Josephson current,

$$I_{L,n} = I_J \sin\left[\frac{\Phi_n}{\varphi_0}\right], \tag{4}$$

where I_J is the critical Josephson current and $\varphi_0 = \Phi_0/(2\pi)$ is the reduced flux quantum. Here $\Phi_0 = h/(2e)$ where h is Planck constant and e is the electron charge. Differentiation of

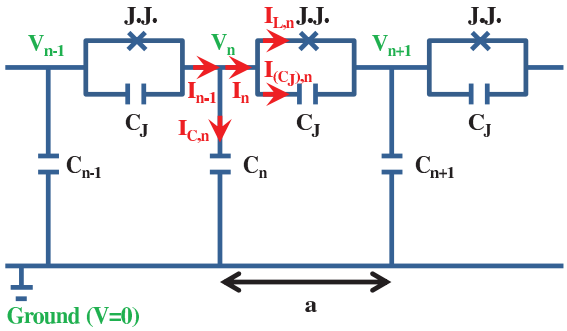

FIG. 1. (Color online) Transmission line scheme. The Josephson junctions and the capacitors are represented by $J.J.$ and C, respectively. The voltages and the currents are denoted by V and I, respectively. The length of all the cells is constant and is equal to a.

the last equation yields

$$\frac{dI_{L,n}}{d\tilde{t}} = \frac{I_J}{\varphi_0}\left(\cos\left[\frac{\Phi_n}{\varphi_0}\right]\right)\frac{d\Phi_n}{d\tilde{t}}. \tag{5}$$

Then,

$$\frac{d\Phi_n}{d\tilde{t}} = \frac{dI_{L,n}}{d\tilde{t}}\frac{\varphi_0}{I_J}\left(1-\sin^2\left[\frac{\Phi_n}{\varphi_0}\right]\right)^{-\frac{1}{2}}, \tag{6}$$

which, upon using Eq. (4), becomes

$$\frac{d\Phi_n}{d\tilde{t}} = \frac{\varphi_0}{I_J}\left(1-\left[\frac{I_{L,n}}{I_J}\right]^2\right)^{-\frac{1}{2}}\frac{dI_{L,n}}{d\tilde{t}}. \tag{7}$$

For a weak nonlinearity, $I_{L,n}/I_J \ll 1$, we approximate

$$\frac{d\Phi_n}{d\tilde{t}} = \frac{\varphi_0}{I_J}\left(1+\frac{1}{2}\left[\frac{I_{L,n}}{I_J}\right]^2\right)\frac{dI_{L,n}}{d\tilde{t}}. \tag{8}$$

Since the current through capacitor C_n is

$$I_{C,n} = -C_n\frac{d}{d\tilde{t}}(0-V_n) + \frac{V_n}{R_n} = C_n\frac{dV_n}{d\tilde{t}} + \frac{V_n}{R_n}, \tag{9}$$

current conservation yields

$$I_n - I_{n-1} = -C_n\frac{dV_n}{d\tilde{t}} - \frac{V_n}{R_n}. \tag{10}$$

Here R_n is the intrinsic (parallel) resistivity of capacitor C_n, accounting for dielectric loss in a realistic capacitor. Next, we use Eqs. (3) and (8) to get

$$V_{n+1} - V_n = -L\frac{dI_{L,n}}{d\tilde{t}} - \frac{\varphi_0}{6I_J^3}\frac{d}{d\tilde{t}}(I_{L,n})^3, \tag{11}$$

where $L = \varphi_0/I_J$. Introducing the node fluxes $\tilde{\varphi}_n$ via

$$V_n \equiv \frac{d\tilde{\varphi}_n}{d\tilde{t}}, \tag{12}$$

and integrating (11), we obtain

$$\tilde{\varphi}_{n+1} - \tilde{\varphi}_n = -LI_{L,n} - \frac{\varphi_0}{6I_J^3}I_{L,n}^3, \tag{13}$$

where, being interested in oscillatory solutions, we set the integration constant to zero. The last equation yields

$$I_{L,n} = -\frac{1}{L}(\tilde{\varphi}_{n+1} - \tilde{\varphi}_n) - \frac{\varphi_0}{6I_J^3L}I_{L,n}^3. \tag{14}$$

Here, assuming that the nonlinear term is small, we can approximate to lowest (nonlinear) order:

$$I_{L,n} \approx -\frac{1}{L}(\tilde{\varphi}_{n+1} - \tilde{\varphi}_n). \tag{15}$$

Then, to next order,

$$I_{L,n} = -\frac{1}{L}(\tilde{\varphi}_{n+1} - \tilde{\varphi}_n) + \frac{\varphi_0}{6I_J^3L^4}(\tilde{\varphi}_{n+1} - \tilde{\varphi}_n)^3. \tag{16}$$

Finally, combining Eqs. (1), (2), (10), (12), and (16), we obtain the weakly nonlinear system describing our transmission line,

$$\begin{aligned} -C_n\frac{d^2\tilde{\varphi}_n}{d\tilde{t}^2} &= -C_J\frac{d^2}{d\tilde{t}^2}[\tilde{\varphi}_{n+1} + \tilde{\varphi}_{n-1} - 2\tilde{\varphi}_n] \\ &\quad - \frac{1}{L}[\tilde{\varphi}_{n+1} + \tilde{\varphi}_{n-1} - 2\tilde{\varphi}_n] \\ &\quad + \frac{\varphi_0}{6I_J^3L^4}[(\tilde{\varphi}_{n+1} - \tilde{\varphi}_n)^3 - (\tilde{\varphi}_n - \tilde{\varphi}_{n-1})^3] \\ &\quad + \frac{1}{R_n}\frac{d\tilde{\varphi}_n}{d\tilde{t}}. \end{aligned} \tag{17}$$

At this stage, assuming a sufficiently long wavelength λ of a wave-type excitation of the chain ($a/\lambda \ll 1$), we use the continuum approximation and replace the discrete n by a continuous position $\tilde{x}$ along the line and replace the finite differences in the discrete line equations by their continuous counterparts to second order in (a/λ):

$$\tilde{\varphi}_{n+1} - \tilde{\varphi}_n \approx a\frac{\partial\tilde{\varphi}}{\partial\tilde{x}} + \frac{1}{2}a^2\frac{\partial^2\tilde{\varphi}}{\partial\tilde{x}^2}, \tag{18}$$

$$\tilde{\varphi}_n - \tilde{\varphi}_{n-1} \approx a\frac{\partial\tilde{\varphi}}{\partial\tilde{x}} - \frac{1}{2}a^2\frac{\partial^2\tilde{\varphi}}{\partial\tilde{x}^2}, \tag{19}$$

$$\tilde{\varphi}_{n+1} + \tilde{\varphi}_{n-1} - 2\tilde{\varphi}_n \approx a^2\frac{\partial^2\tilde{\varphi}}{\partial\tilde{x}^2}. \tag{20}$$

Then, to lowest significant order in (a/λ),

$$(\tilde{\varphi}_{n+1} - \tilde{\varphi}_n)^3 - (\tilde{\varphi}_n - \tilde{\varphi}_{n-1})^3 \approx 3a^4\left(\frac{\partial^2\tilde{\varphi}}{\partial\tilde{x}^2}\right)\left(\frac{\partial\tilde{\varphi}}{\partial\tilde{x}}\right)^2, \tag{21}$$

and, thus, the continuous counterpart of (17) becomes

$$\begin{aligned} &C\frac{\partial^2\tilde{\varphi}}{\partial\tilde{t}^2} - \frac{a^2}{L}\frac{\partial^2\tilde{\varphi}}{\partial\tilde{x}^2} - C_Ja^2\frac{\partial^4\tilde{\varphi}}{\partial\tilde{t}^2\partial\tilde{x}^2} + \frac{\varphi_0a^4}{2I_J^3L^4}\left(\frac{\partial^2\tilde{\varphi}}{\partial\tilde{x}^2}\right)\left(\frac{\partial\tilde{\varphi}}{\partial\tilde{x}}\right)^2 \\ &\quad + \frac{1}{R}\frac{d\tilde{\varphi}}{d\tilde{t}} = 0. \end{aligned} \tag{22}$$

In this weakly nonlinear wave equation, the first three terms describe weakly dispersive linear waves with spatially dependent phase velocity, while the fourth and fifth terms represent the nonlinearity and dissipation in the problem. We will show below that it is the combination of the weak dispersion and cubic nonlinearity which allows efficient parametric amplification in the system via the four-wave mixing process.

In the following, we use dimensionless time $t = \tilde{t}(LC_J)^{-1/2}$ and coordinate $x = \tilde{x}/a$, and seek solutions for

the wave equation as a superposition of three waves (pump, signal, and idler):

$$\tilde{\varphi}(x,t) = \tfrac{1}{2}[\tilde{A}_p(x)e^{i\psi_p} + \tilde{A}_s(x)e^{i\psi_s} + \tilde{A}_i(x)e^{i\psi_i} + \text{c.c.}], \tag{23}$$

where c.c. denotes complex conjugate. We define the dimensionless wave vectors and constant frequencies of the waves as $k_m(x) = \partial\psi_m/\partial x$ and $\omega_m = -\partial\psi_m/\partial t$, respectively. In our analysis, we assume the frequency matching condition of a degenerate four-wave mixing process,

$$\omega_s + \omega_i = 2\omega_p. \tag{24}$$

In the Appendix, we derive from Eq. (22) a dimensionless wave equation,

$$\frac{\partial^2\varphi}{\partial x^2} + \frac{\partial^4\varphi}{\partial x^2\partial t^2} - \rho(x)\frac{\partial^2\varphi}{\partial t^2} - \nu(x)\frac{\partial\varphi}{\partial t} = \gamma\frac{\partial}{\partial x}\left[\left(\frac{\partial\varphi}{\partial x}\right)^3\right]. \tag{25}$$

Here $\varphi = \omega_p\tilde{\varphi}/(LI_J)$ is a dimensionless node flux,

$$\rho = \frac{C(x)}{C_J}, \quad \nu = \rho(x)\frac{\sqrt{LC_J}}{RC}, \quad \gamma = \frac{\varphi_0}{6I_JL\omega_p^2}, \tag{26}$$

and RC is a constant since both R and C are defined by the area of the capacitors. We also derive there a set of three evolution equations for the normalized complex envelope amplitudes,

$$a_m \equiv \frac{u_m\omega_p\sqrt{k_m(x)}}{LI_J}\tilde{A}_m, \tag{27}$$

where $u_m \equiv (1-\omega_m^2)^{1/2}$. The equations for a_m are

$$\frac{da_p}{dx} + \frac{\nu_p}{2}a_p - i\frac{3\gamma}{8}\tilde{k}_p(\tilde{k}_p|a_p|^2 + 2\tilde{k}_s|a_s|^2 + 2\tilde{k}_i|a_i|^2)a_p = i\mu a_p^* a_s a_i e^{i\Psi}, \tag{28}$$

$$\frac{da_s}{dx} + \frac{\nu_s}{2}a_s - i\frac{3\gamma}{8}\tilde{k}_s(2\tilde{k}_p|a_p|^2 + \tilde{k}_s|a_s|^2 + 2\tilde{k}_i|a_i|^2)a_s = i\mu a_p^2 a_i^* e^{-i\Psi}, \tag{29}$$

$$\frac{da_i}{dx} + \frac{\nu_i}{2}a_i - i\frac{3\gamma}{8}\tilde{k}_i(2\tilde{k}_p|a_p|^2 + 2\tilde{k}_s|a_s|^2 + \tilde{k}_i|a_i|^2)a_i = i\mu a_p^2 a_s^* e^{-i\Psi}, \tag{30}$$

where

$$\tilde{k}_m \equiv \frac{k_m}{u_m^2}, \quad \nu_m \equiv \frac{\omega_m\nu}{k_m u_m^2}, \quad \mu = \frac{3\gamma}{4}\tilde{k}_p(\tilde{k}_s\tilde{k}_i)^{1/2}. \tag{31}$$

In the next section, we will find an analytical closed-form solution for the envelope equations under certain conditions, and compare it to the numerical solution of these equations.

III. STRONG PUMP APPROXIMATION

In this section we discuss the dynamics of our system in the case $|a_{s,i}| \ll |a_p|$, when the pump depletion due to the coupling to the signal and the idler can be neglected. We limit the analysis to a uniform transmission line with ρ and k_m constant. We neglect the dissipation effect at this stage, i.e., set $\nu_m = 0$. We also neglect the quadratic terms in $a_{s,i}$ in Eqs. (28)–(30), yielding the system,

$$\frac{da_p}{dx} - ir_p|a_p|^2a_p = 0, \tag{32}$$

$$\frac{da_s}{dx} - ir_s|a_p|^2a_s = i\mu a_p^2 a_i^* e^{-i\Psi}, \tag{33}$$

$$\frac{da_i}{dx} - ir_i|a_p|^2a_i = i\mu a_p^2 a_s^* e^{-i\Psi}, \tag{34}$$

where $r_p \equiv 3\gamma\tilde{k}_p^2/8$ and $r_{s,i} \equiv 3\gamma\tilde{k}_p\tilde{k}_{s,i}/4$. The equation for the pump is now decoupled and yields the solution,

$$a_p = B_{p,0}e^{i\theta_p(x)}, \tag{35}$$

where $B_{p,0}$ is the real amplitude of the initial condition $a_{p,0} = B_{p,0}e^{i\theta_{p,0}}$ and $\theta_p(x) = \theta_{p,0} + r_pB_{p,0}^2x$ (throughout this paper, the subscript "0" denotes the initial condition value). Then, Eqs. (33) and (34) become

$$\frac{d\tilde{a}_s}{dx} + i\left[(r_p - r_s)B_{p,0}^2 - \frac{\Delta k}{2}\right]\tilde{a}_s = i\mu B_{p,0}^2\hat{a}_i, \tag{36}$$

$$\frac{d\hat{a}_i}{dx} - i\left[(r_p - r_i)B_{p,0}^2 - \frac{\Delta k}{2}\right]\hat{a}_i = -i\mu B_{p,0}^2\tilde{a}_s, \tag{37}$$

where $\tilde{a}_{s,i} = a_{s,i}\exp(-i[\theta_p - \Psi/2])$ and $\hat{a}_i = \tilde{a}_i^*$. To shorten the notations, we write this system as

$$\frac{dy_s}{dx} + i\alpha_s y_s - i\beta y_i = 0, \tag{38}$$

$$\frac{dy_i}{dx} - i\alpha_i y_i + i\beta y_s = 0, \tag{39}$$

where $y_s = \tilde{a}_s$, $y_i = \hat{a}_i$, $\alpha_s = (r_p - r_s)B_{p,0}^2 - \Delta k/2$, $\alpha_i = (r_p - r_i)B_{p,0}^2 - \Delta k/2$, and $\beta = \mu B_{p,0}^2$. These equations can be solved by the usual normal mode analysis. We seek solutions in the form $y_{s,i} \sim e^{ipx}$, yielding an algebraic system,

$$\mathbf{D}\mathbf{y} = \begin{pmatrix} p + \alpha_s & -\beta \\ \beta & p - \alpha_i \end{pmatrix}\begin{pmatrix} y_s \\ y_i \end{pmatrix} = 0. \tag{40}$$

We find p by solving the characteristic equation $\text{Det}(\mathbf{D}) = 0$,

$$p^2 + (\alpha_s - \alpha_i)p + \beta^2 - \alpha_s\alpha_i = 0. \tag{41}$$

This yields two modes:

$$p_\pm = \frac{(\alpha_i - \alpha_s) \pm \sqrt{(\alpha_s + \alpha_i)^2 - 4\beta^2}}{2} = \frac{(\alpha_i - \alpha_s)}{2} \pm \sqrt{\Delta_p}, \tag{42}$$

where

$$\Delta_p = [(\alpha_s + \alpha_i)^2/4] - \beta^2. \tag{43}$$

The general solution of Eqs. (38) and (39) is a sum of two independent solutions $\mathbf{y}_\pm$:

$$\mathbf{y} = \begin{pmatrix} y_s \\ y_i \end{pmatrix} = \mathbf{y}_+ + \mathbf{y}_- = \mathbf{y}_{+,0}e^{ip_+x} + \mathbf{y}_{-,0}e^{ip_-x}, \tag{44}$$

where

$$\mathbf{D}(p_+)\mathbf{y}_+ = \mathbf{D}(p_-)\mathbf{y}_- = 0, \tag{45}$$

leading to relations between the components of the vectors $\mathbf{y}_+$ and $\mathbf{y}_-$. Then the general solution at the initial stage is

$$\begin{pmatrix} y_s \\ y_i \end{pmatrix} = \begin{pmatrix} 1 \\ \sigma/\beta \end{pmatrix}c_+e^{ip_+x} + \begin{pmatrix} \sigma/\beta \\ 1 \end{pmatrix}c_-e^{ip_-x}, \tag{46}$$

where

$$\sigma = \frac{\alpha_s + \alpha_i}{2} + \sqrt{\Delta_p}. \tag{47}$$

The coefficients $c_\pm$ are found from the initial conditions,

$$c_+ + \frac{\sigma}{\beta} c_- = y_{s,0}, \tag{48}$$

$$\frac{\sigma}{\beta} c_+ + c_- = y_{i,0}, \tag{49}$$

i.e.,

$$\begin{pmatrix} c_+ \\ c_- \end{pmatrix} = \frac{\beta}{\beta^2 - \sigma^2} \begin{pmatrix} \beta y_{s,0} - \sigma y_{i,0} \\ \beta y_{i,0} - \sigma y_{s,0} \end{pmatrix}. \tag{50}$$

At this point we can derive a simple expression for the signal power gain $G_s = (B_s/B_{s,0})^2$. Assuming that the initial amplitude of the idler is negligible comparing to the initial signal amplitude $|y_{i,0}/y_{s,0}| \ll 1$ and substituting Eq. (50) into Eq. (46) yields an approximate expression for $B_s/B_{s,0} = |y_s|/B_{s,0}$ from which we find that

$$G_s \approx \left| \frac{\beta^2 e^{ip_+ x} - \sigma^2 e^{ip_- x}}{\beta^2 - \sigma^2} \right|^2. \tag{51}$$

Due to our assumptions of strong pump and negligible dissipation, the corresponding expression of the pump gain $G_p = (B_p/B_{p,0})^2$ is equal to 0.

The amplification bandwidth in the problem is the spectral range where $\Delta_p < 0$. Substituting the definitions of α_s, α_i, β, and r_m into the expression for Δ_p, Eq. (43) yields

$$\begin{aligned} \Delta_p &= \frac{(\alpha_s + \alpha_i)^2}{4} - \beta^2 \\ &= \frac{\left[(2r_p - r_s - r_i)B_{p,0}^2 - \Delta k\right]^2}{4} - \mu^2 B_{p,0}^4. \end{aligned} \tag{52}$$

The boundaries of the amplification bandwidth are determined by setting $\Delta_p = 0$. This yields the bandwidth in terms of the wave vectors mismatch

$$\Delta k_B = (2r_p - r_s - r_i \pm 2\mu)B_{p,0}^2, \tag{53}$$

or by using the definitions of r_m and μ,

$$\Delta k_B = \tfrac{3}{4}\gamma \tilde{k}_p B_{p,0}^2 [\tilde{k}_p - \tilde{k}_s - \tilde{k}_i \pm 2(\tilde{k}_s \tilde{k}_i)^{1/2}]. \tag{54}$$

On the other hand, $\tilde{k}_p - \tilde{k}_s - \tilde{k}_i = -\tilde{k}_p - \Delta\tilde{k} \approx -\tilde{k}_p - 3\Delta k$, and we can rewrite the last expression as

$$\Delta k_B \left[1 + \tfrac{9}{4}\gamma \tilde{k}_p B_{p,0}^2\right] = \tfrac{3}{4}\gamma \tilde{k}_p B_{p,0}^2 [-\tilde{k}_p + 2(\tilde{k}_s \tilde{k}_i)^{1/2}], \tag{55}$$

where we have left the positive sign in (54) for having $\Delta k_B > 0$ in agreement with Eq. (A32). Finally, we approximate $\tilde{k}_m \approx k_m$ in the right-hand side of the last equation, neglect the small term with γ in the left-hand side, and use the previously shown relation $\Delta k \approx 3k_p(\Delta\omega)^2$ [Eq. (A32)] to obtain an estimate for the amplification bandwidth in terms of the frequencies,

$$|\Delta\omega_B| = |\omega_s - \omega_p| \approx \tfrac{1}{2}(\gamma k_p)^{1/2} B_{p,0}. \tag{56}$$

Within this bandwidth, the imaginary part of p_- is negative, therefore, the second term in Eq. (46) grows exponentially. The spatial exponential gain factor is $g = \sqrt{-\Delta_p}$. The gain vanishes at the frequency shifts given in Eq. (56) and reaches the maximum value at $\omega_s = \omega_p$, i.e., in the center of the amplification band. This maximal exponential gain factor is

$$g_{\max} = \sqrt{\frac{3}{4}}\mu_p B_{p,0}^2 \approx \left(\frac{3}{4}\right)^{3/2} \gamma \tilde{k}_p^2 B_{p,0}^2, \tag{57}$$

where μ_p is μ at $\omega_s = \omega_p$.

It is interesting to compare between the gain profile in the process of degenerate four-wave mixing in our present system and in the related well-known process in third-order $\chi^{(3)}$ nonlinear optical medium.[19] In our present system we see from Eq. (A32) that the maximal gain occurs at the condition of perfect wave vectors matching $\Delta k = 0$. On the contrary, in a $\chi^{(3)}$ optical medium, the maximal gain occurs in a nonvanishing value of Δk that is proportional to the initial pump power P_0 (see p. 396 of Ref. 19). However, in both types of processes, the bandwidth Δk_B in which the gain is positive is proportional to the product γP_0 where γ is the relevant nonlinear coupling coefficient [see Eq. (53)].

Finally, we discuss the evolution of the phase mismatch between the waves. Using the representation $a_m = B_m e^{i\theta_m}$ where B_m and θ_m are real, and defining the phase mismatch $\Theta \equiv \theta_s + \theta_i - 2\theta_p + \Psi$, we find that in the Appendix a set of four evolution equations for the B_m and Θ. In the linear stage, without dissipation, Eqs. (A25) and (A26) in the Appendix can be approximated by

$$\frac{dB_s}{dx} = \mu B_p^2 B_i \sin\Theta, \tag{58}$$

$$\frac{dB_i}{dx} = \mu B_p^2 B_s \sin\Theta. \tag{59}$$

These equations can be used to write

$$\sin\Theta = \frac{B_s \frac{dB_s}{dx} + B_i \frac{dB_i}{dx}}{2\mu B_p^2 B_s B_i}. \tag{60}$$

Within the amplification bandwidth, $\Delta_p < 0$, and the first (exponentially decaying) term in the solution Eq. (46) is negligible at locations such that $gx \gg 1$. In this regime, $dB_{s,i}/dx \approx g B_{s,i}$ and $B_s \approx B_i$, so we obtain

$$\sin\Theta \to \frac{g}{\mu B_{p,0}^2}, \tag{61}$$

i.e., Θ approaches a constant value,

$$\Theta_\infty = \pi - \arcsin\left(\frac{g}{\mu B_{p,0}^2}\right). \tag{62}$$

Note that in choosing between the two possible solutions of Θ_∞, we take the one with $\cos\Theta_\infty < 0$. This choice is explained by examining the approximation of Eq. (A31) in the linear regime:

$$\begin{aligned} \frac{d\Theta}{dx} &= \Delta k + \frac{3\gamma}{4}\tilde{k}_p B_{p,0}^2 (\Delta\tilde{k} + \tilde{k}_p) \\ &\quad + \mu B_{p,0}^2 \left(\frac{B_i}{B_s} + \frac{B_s}{B_i}\right) \cos\Theta. \end{aligned} \tag{63}$$

Since Δk and $\Delta\tilde{k}$ are non-negative, a constant solution $\Theta = \Theta_\infty$ can be reached for $\cos\Theta_\infty < 0$ only.

At this stage, we present some numerical results for a typical set of parameters, and compare these results with our analytical results. We used the following parameters in our calculations: $\varphi_0 = 3.29 \times 10^{-16}$ Wb, $C = 4.51 \times 10^{-14}$ F, $C_J = 3.29 \times 10^{-13}$ F, $I_J = 3.29$ μA, $RC = \infty$, $f_p = \omega_p/2\pi = 6$ GHz, $\tilde{A}_{p,0} = 2.18 \times 10^{-15}$ V $\times$ s, $\tilde{A}_{s,0}/\tilde{A}_{p,0} = 9.3 \times 10^{-5}$, $\tilde{A}_{i,0}/\tilde{A}_{p,0} = 1.09 \times 10^{-8}$, $\Psi_0 = 0$, and $\theta_p = \theta_s = \theta_i = 0$. For signal and idler frequencies $f_s = \omega_s/2\pi = 7$ GHz and $f_i = 2f_p - f_s = 5$ GHz, this set of physical parameters is reduced to the following set of normalized parameters: $\mu = 0.0195$, $\nu_p = \nu_s = \nu_i = 0$, $B_{p,0} = 0.4$, $B_{s,0}/B_{p,0} = 10^{-4}$, $B_{i,0}/B_{p,0} = 10^{-8}$, and $\Theta_0 = 0$. The solution of the normalized wave powers and the phase Θ are presented in Figs. 2(a) and 2(b), respectively. Excellent agreement is seen between the numerical solution of Eqs. (A24)–(A26), and (A31) and the analytic solution Eqs. (35) and (46). As predicted, the numerical value of Θ approaches the asymptotic value Θ_∞, given by Eq. (62). As predicted for $x \gg 1/g = 389$, the dependence of the wave amplitudes on the position is exponential.

Using our previous definitions, the voltage and the current were calculated at $x = 0$ and $x = 2000$ (the line input and output). From these quantities, the absolute value of the impedance of the pumped line was found to be equal to 50 Ω with negligible phase shift between the voltage and the current phases. For comparison, the linear impedance on the line (without pumping) is equal to $(L/C)^{1/2} = 47.1$ Ω. Figure 3 shows the numerical solution for the signal gain compared with the analytical solution Eq. (51). The results are plotted for various values of initial reduced pump amplitude, $B_{p,0} = 0.4$ (used in Fig. 2) as well as lower values of $B_{p,0} = 0.2$ and $B_{p,0} = 0.3$. All the rest of the parameters are the same as in Fig. 2. We see again that there is excellent agreement between the solutions and the corresponding curves are overlapping. It is seen that the gain is a monotonically increasing function of position with magnitude that increases as a function of the initial pump amplitude. It is worth noting that in a real device, the amplifier will be exposed to quantum vacuum fluctuations at its input across the entire band of amplification. These fluctuations will be amplified along with any signal present at the input, using some of the power of the pump power. Hence, as the gain of the device grows, the pump will be depleted, and the actual signal gain may be lower than what is presented in Fig. 3. Figure 4 shows the local signal gain calculated by analytical solution Eq. (51) as a function of the signal frequency f_s. We see that the maximal signal gain decreases as the signal frequency becomes farther from the pump frequency. The black line is located where the signal gain level is 3 dB below the local peak, indicating the useful amplification bandwidth. Note that for larger values of x, the signal gain increases but the bandwidth decreases. Figure 5 shows the exponential gain factor $g = (-\Delta_p)^{1/2}$ as a function of the signal frequency. The amplification bandwidth lies approximately between 3.4 and 8.6 GHz and the maximal gain is obtained at $f_s = f_p$ and is equal to 2.74×10^{-3}. Figure 6 shows the same solution as in Fig. 2, but for larger x. One can see that for $x > 3400$, the difference between the analytical solution and the numerical solution becomes considerable. This is a consequence of the violation of the strong pump approximation. One can also see that the numerical solution of the equations for large x exhibits periodic oscillations of the phase Θ accompanied by a periodic exchange of energy between the waves. This behavior is characteristic of many other wave mixing processes, e.g., in the context of nonlinear optics.[20]

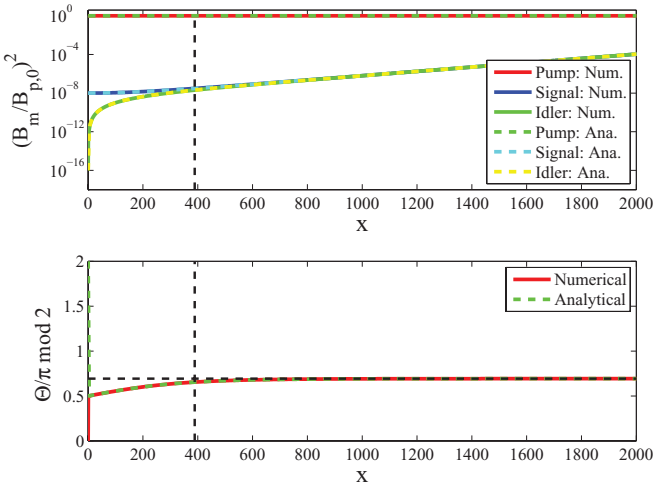

FIG. 2. (Color online) Evolution of (a) the normalized power of the pump wave B_p^2, signal wave B_s^2, and idler wave B_i^2, and (b) the phase mismatch Θ versus normalized position along the transmission line. The numerical solution of Eqs. (A24)–(A26), and (A31) and the analytical solution Eqs. (35) and (46) are plotted by solid lines and dashed lines, respectively. Note that the corresponding numerical and analytical curves are overlapping. The vertical dashed line is located in the point $x = 1/g$ after which the wave amplitudes grow exponentially with exponent g. The asymptotic value of the phase Θ_∞ expressed by Eq. (62) is plotted by a horizontal dashed line in Fig. 2(b).

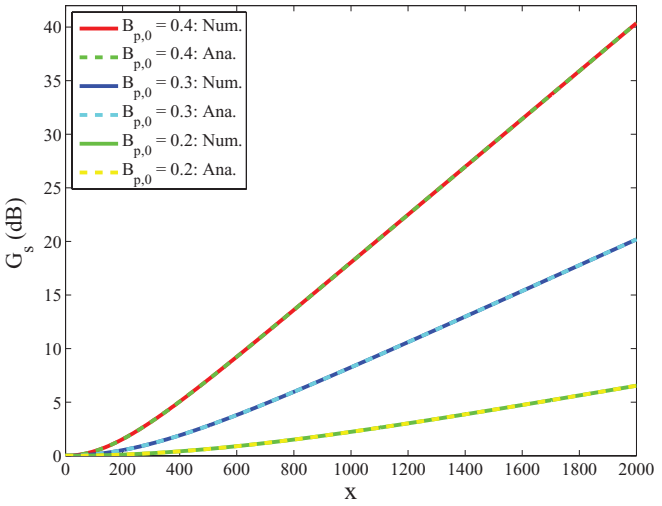

FIG. 3. (Color online) Signal power gain in the system for the case of Fig. 2 ($B_{p,0} = 0.4$) as well as for lower initial pump amplitudes $B_{p,0} = 0.2$ and 0.3. The numerical solution calculated from the solution of Eqs. (A24)–(A26) and (A31) and the analytical solution Eq. (51) are plotted by solid lines and dashed lines, respectively. Note that the corresponding numerical and analytical curves are overlapping.

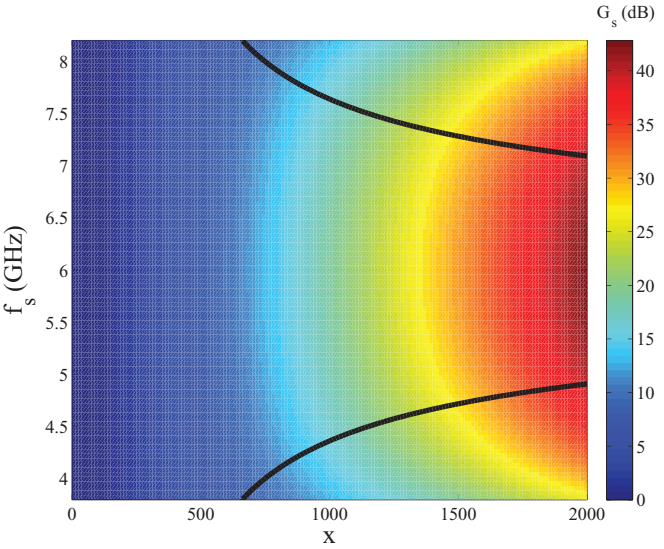

FIG. 4. (Color online) Signal power gain as a function of signal frequency and position given by the analytical expression Eq. (51). All the parameters are the same as in Fig. 2 except the varying signal frequency. The black line is located where the gain level is 3 dB below the local peak.

IV. SUMMARY

We have used a long wavelength approximation to derive a nonlinear wave equation characterizing a transmission line composed of capacitively shunted Josephson junctions. The analysis of this wave equation shows that traveling waves copropagating along the line may interact via four-wave mixing. We have studied analytically and numerically the process of degenerate four-wave mixing in which $f_s + f_i = 2f_p$, where $f_{p,s,i}$ denote the frequency of the pump, signal, and idler, respectively.

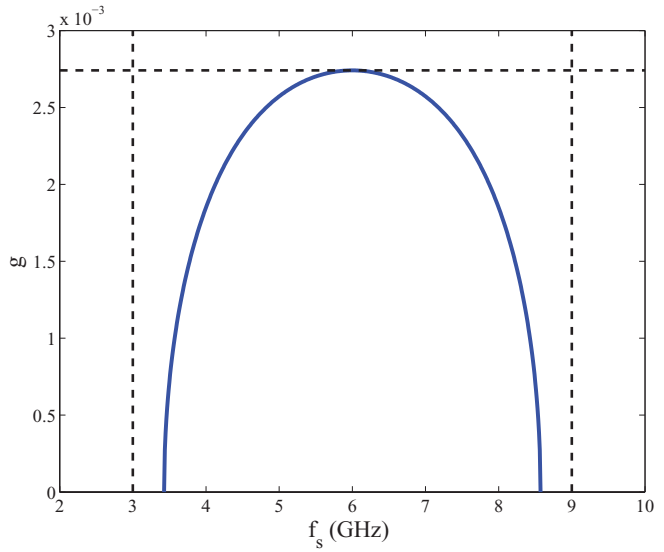

FIG. 5. (Color online) Exponential gain factor $g = \sqrt{-\Delta_p}$ versus signal frequency [given by Eq. (52)]. The maximal gain is obtained at $f_s = f_p$. The approximate value $g_{\max}$ given by Eq. (57) is plotted by a horizontal dashed line. The simplified expression for the amplification bandwidth for which $g > 0$, given by Eq. (56) is plotted by vertical dashed lines.

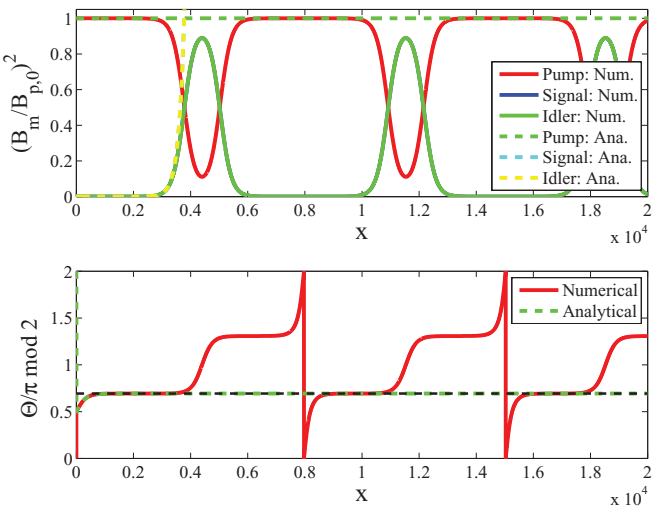

FIG. 6. (Color online) Spatial evolution of the system for the same case of Fig. 2 in long distance. In long distance, in which the amplified signal becomes large, the underlying assumption of the analytical solution derivation fails, and the analytical solution becomes invalid.

Under the assumption of the strong pump approximation, we have derived closed-form expressions for the following quantities: (a) the normalized amplitudes of the interacting waves B_m, Eqs. (35) and (46); (b) the signal power gain G_s, Eq. (51); (c) the exponential gain factor $g = \sqrt{-\Delta_p}$, Eq. (52); (d) the amplification bandwidth for which $g > 0$, Eq. (56); (e) the maximal exponential gain factor $g_{\max}$, Eq. (57).

We have found that degenerate four-wave mixing in the considered system can lead to efficient parametric amplification in a wide spectral bandwidth (3.4–8.6 GHz for typical parameters). Such a wide-band, transmission-geometry amplifier would be of interest in experiments on microwave quantum optics and quantum circuit readout near the quantum limit. In particular, the transmission geometry realized by this design would in principle remove the need for microwave circulators between the system under measurement and the first-stage amplifier. This would enable pursuit of a fully quantum limited measurement apparatus on a single chip incorporating both the quantum system of interest and the quantum-limited following amplifier, substantially reducing losses between the two. The large bandwidth and dynamic range also make it a good candidate for a low-noise second-stage following amplifier, possibly supplementing or replacing conventional high- electron-mobility transistor (HEMT) amplifiers. Such an amplifier could also prove useful as a low-power device for satellite-based wide-band microwave communication.

ACKNOWLEDGMENTS

The authors thank O. Naaman, D. H. Slichter, K. Murch, and R. Vijay for helpful discussions. Financial support is acknowledged from HYPRES Inc. (US Army Small Business Innovation Research program), the Office of Naval Research, and the Israel Science Foundation (Grant No. 451/10).

APPENDIX: ENVELOPE EQUATIONS

In this appendix we derive a set of three differential equations for the complex envelopes of the pump, signal, and idler waves. From the equations for the complex envelopes, we then derive a set of four differential equations for the real amplitudes of the waves and the phase mismatch between phases of the three interacting waves. We start by rewriting our wave equation (22) as

$$\frac{\partial^2\tilde{\varphi}}{\partial x^2}+\frac{\partial^4\tilde{\varphi}}{\partial x^2\partial t^2}-\rho(x)\frac{\partial^2\tilde{\varphi}}{\partial t^2}-\nu(x)\frac{\partial\tilde{\varphi}}{\partial t}=\tilde{\gamma}\frac{\partial}{\partial x}\left[\left(\frac{\partial\tilde{\varphi}}{\partial x}\right)^3\right], \tag{A1}$$

where $t=\tilde{t}(LC_J)^{-1/2}$ and coordinate $x=\tilde{x}/a$ are dimensionless time and coordinate, respectively,

$$\rho=\frac{C(x)}{C_J},\quad \nu=\rho(x)\frac{\sqrt{LC_J}}{RC},\quad \tilde{\gamma}=\frac{\varphi_0}{6I_J^3L^3}, \tag{A2}$$

and RC is a constant since both R and C are defined by the area of the capacitors. Next, we seek solutions as a superposition of three waves (pump, signal, and idler):

$$\tilde{\varphi}(x,t)=\tfrac{1}{2}[\tilde{A}_p(x)e^{i\psi_p}+\tilde{A}_s(x)e^{i\psi_s}+\tilde{A}_i(x)e^{i\psi_i}+\text{c.c.}], \tag{A3}$$

where c.c. denotes complex conjugate. We define the dimensionless wave vectors and constant frequencies of the waves as $k_m(x)=\partial\psi_m/\partial x$ and $\omega_m=-\partial\psi_m/\partial t$, respectively. Furthermore, we assume the frequency matching condition of a degenerate four-wave mixing process:

$$\omega_s+\omega_i=2\omega_p, \tag{A4}$$

and relate k_m and ω_m via the local linear dispersion relations (without dissipation):

$$k_m^2(x)=\frac{\rho(x)\omega_m^2}{1-\omega_m^2},\quad m=\{p,s,i\}. \tag{A5}$$

First, we rescale $\tilde{\varphi}$ to adjust it to our physical problem. We assume that $\rho(x)\sim O(1)$ and that the dimensionless wave vector $k_m\ll 1$ (long wavelength excitation). Then $\omega_m\ll 1$ [see Eq. (A5)] and $\omega_m\approx k_m$. Furthermore, Eq. (13) yields $\partial\tilde{\varphi}/\partial x\approx -LI_L$ and, thus, in orders of magnitude,

$$\tilde{\varphi}\sim\frac{LI_J}{k}\frac{I_L}{I_J}\approx\frac{LI_J}{\omega}\frac{I_L}{I_J}. \tag{A6}$$

This suggests rescaling $\tilde{\varphi}$ as

$$\varphi=\frac{\omega_p\tilde{\varphi}}{LI_J}, \tag{A7}$$

where we use the dimensionless frequency of the pump for definiteness. Note that this dimensionless φ roughly represents I_L in units of I_J. For example, for the pump wave $\varphi_p\sim I_{Lp}/I_J$, which must be sufficiently small in our weakly nonlinear theory. Similarly, we define the dimensionless wave amplitudes $A_m=\omega_p\tilde{A}_m/(LI_J)$. We will assume that the rescaled pump wave amplitude is bounded by 0.5 in the following. The above rescaling of φ does not change the form of (A1) but now the coupling coefficient becomes

$$\gamma=\left(\frac{LI_J}{\omega_p}\right)^2\tilde{\gamma}=\frac{\varphi_0}{6I_JL\omega_p^2}, \tag{A8}$$

and the dimensionless wave equation is

$$\frac{\partial^2\varphi}{\partial x^2}+\frac{\partial^4\varphi}{\partial x^2\partial t^2}-\rho(x)\frac{\partial^2\varphi}{\partial t^2}-\nu(x)\frac{\partial\varphi}{\partial t}=\gamma\frac{\partial}{\partial x}\left[\left(\frac{\partial\varphi}{\partial x}\right)^3\right]. \tag{A9}$$

Substitution of Eq. (A3) into Eq. (A9) and the neglect of d^2A_m/dx^2 (the WKB approximation) yields the following linear parts of Eq. (A9) for each of the interacting waves:

$$\mathcal{L}\left(\frac{1}{2}A_me^{i\psi_m}\right)\approx\frac{1}{2}\left[(1-\omega_m^2)\left(2ik_m\frac{d}{dx}+i\frac{dk_m}{dx}\right)+i\omega_m\nu\right]A_me^{i\psi_m}+\text{c.c.}. \tag{A10}$$

Next, we proceed to the calculation of the nonlinear part, the right-hand side of Eq. (A9). We focus on the degenerate resonant four-wave mixing in which the following phase mismatch:

$$\Psi\equiv\psi_s+\psi_i-2\psi_p, \tag{A11}$$

is approximately constant. Consequently, after substitution of (A3) in Eq. (A9), we leave only resonant terms in the nonlinear terms for each of the interacting waves (those that are oscillating in frequency ω_m). We will show now that this results with a set of coupled mode equations in the following form:

$$\mathcal{L}\left(\tfrac{1}{2}A_me^{i\psi_m}\right)=[S_m+Q_me^{i\epsilon_m\Psi}]e^{i\psi_m}+\text{c.c.}, \tag{A12}$$

where $\epsilon_m=+1$ for $m=p$ and $\epsilon_m=-1$ for $m=s,i$. Note that S_m are analogous to the self-phase and cross-phase modulation terms and Q_m are analogous to the mixing terms in the context of nonlinear optics (however, here the form of these terms is more complex due to the coupling through the derivatives of φ and involves also cubic powers of k_m and not only A_m as usually appear in nonlinear optics[19,20]). The explicit evaluation of the nonlinear terms S_m and Q_m is as follows. We first calculate

$$\left(\frac{\partial\varphi}{\partial x}\right)^3=-\frac{i}{8}(k_pA_pe^{i\psi_p}+k_sA_se^{i\psi_s}+k_iA_ie^{i\psi_i}-\text{c.c.})^3=\frac{3i}{8}\left[k_p\left(k_p^2|A_p|^2+2k_s^2|A_s|^2+2k_i^2|A_i|^2\right)A_p+2k_pk_sk_iA_p^*A_sA_ie^{i\Psi}\right]e^{i\psi_p}$$
$$+\frac{3i}{8}\left[k_s\left(2k_p^2|A_p|^2+k_s^2|A_s|^2+2k_i^2|A_i|^2\right)A_s+2k_p^2k_iA_p^2A_i^*e^{-i\Psi}\right]e^{i\psi_s}$$
$$+\frac{3i}{8}\left[k_i\left(2k_p^2|A_p|^2+2k_s^2|A_s|^2+k_i^2|A_i|^2\right)A_i+2k_p^2k_sA_p^2A_s^*e^{-i\Psi}\right]e^{i\psi_i}+\text{nonresonant terms}, \tag{A13}$$

where we wrote explicitly only the terms that multiply $e^{i\psi_m}$. The three lines in (A13) are written in a form identifying the resonant terms for use in the three weakly nonlinear coupled wave equations. We then differentiate (A13) with respect to x (each line

separately) assuming phase locking in the system, $\partial\Psi/\partial x \approx 0$, yielding an approximation,

$$\gamma\frac{\partial}{\partial x}\left(\frac{\partial\varphi}{\partial x}\right)^3 \approx -\frac{3\gamma}{8}\left[k_p^2\left(k_p^2|A_p|^2+2k_s^2|A_s|^2+2k_i^2|A_i|^2\right)A_p+2k_p^2k_sk_iA_p^*A_sA_ie^{i\Psi}\right]e^{i\psi_p}$$
$$-\frac{3\gamma}{8}\left[k_s^2\left(2k_p^2|A_p|^2+k_s^2|A_s|^2+2k_i^2|A_i|^2\right)A_s+2k_p^2k_sk_iA_p^2A_i^*e^{-i\Psi}\right]e^{i\psi_s}$$
$$-\frac{3\gamma}{8}\left[k_i^2\left(2k_p^2|A_p|^2+2k_s^2|A_s|^2+k_i^2|A_i|^2\right)A_i+2k_p^2k_sk_iA_p^2A_s^*e^{-i\Psi}\right]e^{i\psi_i}. \quad \text{(A14)}$$

In combining all the above results, we have the following set of slow coupled mode equations:

$$\left(1-\omega_p^2\right)\left(\frac{dA_p}{dx}+\frac{1}{2k_p}\frac{dk_p}{dx}A_p\right)+\frac{\omega_p\nu}{2k_p}A_p=i\frac{3\gamma}{8}\left[k_p\left(k_p^2|A_p|^2+2k_s^2|A_s|^2+2k_i^2|A_i|^2\right)A_p+2k_pk_sk_iA_p^*A_sA_ie^{i\Psi}\right]. \quad \text{(A15)}$$

$$\left(1-\omega_s^2\right)\left(\frac{dA_s}{dx}+\frac{1}{2k_s}\frac{dk_s}{dx}A_s\right)+\frac{\omega_s\nu}{2k_s}A_s=i\frac{3\gamma}{8}\left[k_s\left(2k_p^2|A_p|^2+k_s^2|A_s|^2+2k_i^2|A_i|^2\right)A_s+2k_p^2k_iA_p^2A_i^*e^{-i\Psi}\right]. \quad \text{(A16)}$$

$$\left(1-\omega_i^2\right)\left(\frac{dA_i}{dx}+\frac{1}{2k_i}\frac{dk_i}{dx}A_i\right)+\frac{\omega_i\nu}{2k_i}A_i=i\frac{3\gamma}{8}\left[k_i\left(2k_p^2|A_p|^2+2k_s^2|A_s|^2+k_i^2|A_i|^2\right)A_i+2k_p^2k_sA_p^2A_s^*e^{-i\Psi}\right]. \quad \text{(A17)}$$

Next, for simplification, we introduce new amplitudes:

$$a_m \equiv u_m\sqrt{k_m(x)}A_m, \quad \text{(A18)}$$

where $u_m \equiv (1-\omega_m^2)^{1/2}$. The equations for a_m are

$$\frac{da_p}{dx}+\frac{\nu_p}{2}a_p-i\frac{3\gamma}{8}\tilde{k}_p(\tilde{k}_p|a_p|^2+2\tilde{k}_s|a_s|^2+2\tilde{k}_i|a_i|^2)a_p$$
$$=i\mu a_p^*a_sa_ie^{i\Psi}, \quad \text{(A19)}$$

$$\frac{da_s}{dx}+\frac{\nu_s}{2}a_s-i\frac{3\gamma}{8}\tilde{k}_s(2\tilde{k}_p|a_p|^2+\tilde{k}_s|a_s|^2+2\tilde{k}_i|a_i|^2)a_s$$
$$=i\mu a_p^2a_i^*e^{-i\Psi}, \quad \text{(A20)}$$

$$\frac{da_i}{dx}+\frac{\nu_i}{2}a_i-i\frac{3\gamma}{8}\tilde{k}_i(2\tilde{k}_p|a_p|^2+2\tilde{k}_s|a_s|^2+\tilde{k}_i|a_i|^2)a_i$$
$$=i\mu a_p^2a_s^*e^{-i\Psi}, \quad \text{(A21)}$$

where

$$\tilde{k}_m \equiv \frac{k_m}{u_m^2}, \quad \nu_m \equiv \frac{\omega_m\nu}{k_mu_m^2}, \quad \mu=\frac{3\gamma}{4}\tilde{k}_p(\tilde{k}_s\tilde{k}_i)^{1/2}. \quad \text{(A22)}$$

These equations show that in the case of $\nu_m=\gamma=0$, the normalized "action fluxes," $|a_m|^2=(1-\omega_m^2)k_m|A_m|^2$, are conserved. If the nonlinear coupling is included (still for $\nu_m=0$), $|a_m|^2$ will satisfy the Manley-Rowe relations, i.e., $|a_p|^2+|a_s|^2$, $|a_p|^2+|a_i|^2$, and $|a_s|^2-|a_i|^2$ are conserved. Finally, we write $a_m=B_m\exp(i\theta_m)$ defining the real amplitudes and complex phases, and introduce the phase mismatch in the problem:

$$\Theta \equiv \theta_s+\theta_i-2\theta_p+\Psi, \quad \text{(A23)}$$

and rewrite Eqs. (A19)–(A21) as a system of six real equations:

$$\frac{dB_p}{dx}=-\mu B_pB_sB_i\sin\Theta-\frac{\nu_p}{2}B_p, \quad \text{(A24)}$$

$$\frac{dB_s}{dx}=\mu B_p^2B_i\sin\Theta-\frac{\nu_s}{2}B_s, \quad \text{(A25)}$$

$$\frac{dB_i}{dx}=\mu B_p^2B_s\sin\Theta-\frac{\nu_i}{2}B_i, \quad \text{(A26)}$$

$$\frac{d\theta_p}{dx}=\frac{3\gamma}{8}\tilde{k}_p\left(\tilde{k}_pB_p^2+2\tilde{k}_sB_s^2+2\tilde{k}_iB_i^2\right)+\mu B_sB_i\cos\Theta, \quad \text{(A27)}$$

$$\frac{d\theta_s}{dx}=\frac{3\gamma}{8}\tilde{k}_s\left(2\tilde{k}_pB_p^2+\tilde{k}_sB_s^2+2\tilde{k}_iB_i^2\right)+\mu\frac{B_p^2B_i}{B_s}\cos\Theta, \quad \text{(A28)}$$

$$\frac{d\theta_i}{dx}=\frac{3\gamma}{8}\tilde{k}_i\left(2\tilde{k}_pB_p^2+2\tilde{k}_sB_s^2+\tilde{k}_iB_i^2\right)+\mu\frac{B_p^2B_s}{B_i}\cos\Theta. \quad \text{(A29)}$$

Then,

$$\frac{d\Theta}{dx}=\frac{d\theta_s}{dx}+\frac{d\theta_i}{dx}-2\frac{d\theta_p}{dx}+\frac{d\Psi}{dx}, \quad \text{(A30)}$$

$$\frac{d\Theta}{dx}=\Delta k+\frac{6\gamma}{8}\Delta\tilde{k}\sum_{m=p,s,i}\tilde{k}_mB_m^2$$
$$+\frac{3\gamma}{8}\left(2\tilde{k}_p^2B_p^2-\tilde{k}_s^2B_s^2-\tilde{k}_i^2B_i^2\right)$$
$$+\mu B_p^2B_sB_i\left[\frac{1}{B_s^2}+\frac{1}{B_i^2}-\frac{2}{B_p^2}\right]\cos\Theta, \quad \text{(A31)}$$

where the wave-vector mismatch is $\Delta k \equiv k_s+k_i-2k_p$ and $\Delta\tilde{k}\equiv\tilde{k}_s+\tilde{k}_i-2\tilde{k}_p$. Equations (A24)–(A26) and (A31) comprise a complete set of four ordinary differential equations for the real amplitudes B_m and the phase mismatch Θ. Note that Δk and $\Delta\tilde{k}$ are non-negative. Indeed, using the dispersion relation (A5) and the frequency matching condition (A4), we find that

$$\Delta k=\rho^{1/2}\left(\frac{\omega_s}{\sqrt{1-\omega_s^2}}+\frac{\omega_i}{\sqrt{1-\omega_i^2}}-\frac{2\omega_p}{\sqrt{1-\omega_p^2}}\right)$$
$$\approx\frac{\rho^{1/2}}{2}\left(\omega_s^3+\omega_i^3-2\omega_p^3\right)$$
$$=3\rho^{1/2}\omega_p(\Delta\omega)^2\approx 3k_p(\Delta\omega)^2\geqslant 0, \quad \text{(A32)}$$

where we defined $\Delta\omega=\omega_s-\omega_p=\omega_p-\omega_i$. Similarly, $\Delta\tilde{k}=3\Delta k$.

*oded.yaakobi@emt.inrs.ca

[1]S. J. Asztalos, G. Carosi, C. Hagmann, D. Kinion, K. van Bibber, M. Hotz, L. J. Rosenberg, G. Rybka, J. Hoskins, J. Hwang, P. Sikivie, D. B. Tanner, R. Bradley, and J. Clarke, Phys. Rev. Lett. **104**, 041301 (2010).

[2]R. Vijay, D. H. Slichter, and I. Siddiqi, Phys. Rev. Lett. **106**, 110502 (2011).

[3]R. Vijay, C. Macklin, D. H. Slichter, S. J. Weber, K. W. Murch, R. Naik, A. N. Korotkov, and I. Siddiqi, Nature (London) **490**, 77 (2012).

[4]M. J. Feldman, P. T. Parrish, and R. Y. Chiao, J. Appl. Phys. **46**, 4031 (1975).

[5]A. H. Silver, D. C. Pridmore-Brown, R. D. Sandell, and J. P. Hurrell, IEEE Trans. Magn. **17**, 412 (1981).

[6]N. Calander, T. Claeson, and S. Rudner, J. Appl. Phys. **53**, 5093 (1982).

[7]A. D. Smith, R. D. Sandell, J. F. Burch, and A. H. Silver, IEEE Trans. Magn. **21**, 1022 (1985).

[8]B. Yurke, L. R. Corruccini, P. G. Kaminsky, L. W. Rupp, A. D. Smith, A. H. Silver, R. W. Simon, and E. A. Whittaker, Phys. Rev. A **39**, 2519 (1989).

[9]M. Hatridge, R. Vijay, D. H. Slichter, J. Clarke, and I. Siddiqi, Phys. Rev. B **83**, 134501 (2011).

[10]M. A. Castellanos-Beltran, K. D. Irwin, L. R. Vale, G. C. Hilton, and K. W. Lehnert, Appl. Supercond., IEEE Trans., **19**, 944 (2009).

[11]N. Bergeal, R. Vijay, V. E. Manucharyan, I. Siddiqi, R. J. Schoelkopf, S. M. Girvin, and M. H. Devoret, Nature Phys. **6**, 296 (2010).

[12]N. Bergeal, F. Schackert, M. Metcalfe, R. Vijay, V. E. Manucharyan, L. Frunzio, D. E. Prober, R. J. Schoelkopf, S. M. Girvin, and M. H. Devoret, Nature (London) **465**, 64 (2010).

[13]N. Roch, E. Flurin, F. Nguyen, P. Morfin, P. Campagne-Ibarcq, M. H. Devoret, and B. Huard, Phys. Rev. Lett. **108**, 147701 (2012).

[14]M. Hatridge, S. Shankar, M. Mirrahimi, F. Schackert, K. Geerlings, T. Brecht, K. M. Sliwa, B. Abdo, L. Frunzio, S. M. Girvin, R. J. Schoelkopf, and M. H. Devoret, Science **339**, 6116 (2013).

[15]M. Sweeny and R. Mahler, IEEE Trans. Magn. **21**, 654 (1985).

[16]H. R. Mohebbi and A. H. Majedi, IEEE Trans. Microwave Theory Tech. **53**, 1865 (2009).

[17]B. Yurke, M. L. Roukes, R. Movshovich, and A. N. Pargellis, Appl. Phys. Lett. **69**, 3078 (1996).

[18]B. Ho Eom, P. K. Day, H. G. LeDuc, and J. Zmuidzinas, Nat. Phys. **8**, 623 (2012).

[19]G. P. Agrawal, *Nonlinear Fiber Optics*, 3rd ed. (Academic Press, San Diego, 2001).

[20]R. B. Boyd, *Nonlinear Optics*, 3rd ed. (Academic Press, San Diego, 2008).